IRSTI 20.23.27

https://doi.org/10.26577/jpcsit2025332



<sup>1</sup>Al-Farabi Kazakh National University, Almaty, Kazakhstan <sup>2</sup>Institute of Information and Computational Technologies, Almaty, Kazakhstan \*e-mail: aisulu.ataniyazova@gmail.com

# SPATIOTEMPORAL ASSESSMENT OF SOIL SALINITY IN IRRIGATED AGRICULTURAL LANDS OF KAZAKHSTAN USING REMOTE SENSING

Abstract. Soil salinization poses a significant threat to agricultural productivity and environmental sustainability, particularly in arid and semi-arid regions. This study presents a comprehensive spatiotemporal analysis of soil salinity dynamics in irrigated lands of Alakol District, Zhetisu Region, Kazakhstan, using multi-temporal Sentinel-2 satellite imagery and the Normalized Difference Salinity Index (NDSI). The analysis covered the 2024 growing season, from March to November, with one cloud-free image selected for each month. NDSI values were calculated monthly and classified into four salinity categories: non-saline, slightly saline, moderately saline, and highly saline. Field sampling at 31 locations provided electrical conductivity (EC) data for validation, enabling comparison between surface reflectance-based salinity estimates and ground measurements. The results demonstrated pronounced seasonal trends: NDSI values were lowest in spring due to leaching by precipitation and early irrigation, gradually increasing through summer as evaporation concentrated salts at the surface, and fluctuating in autumn depending on rainfall and drainage conditions. Spatially, fields situated in topographic depressions or near Lake Alakol exhibited the highest salinity levels, whereas upland areas remained relatively unaffected. Notably, no fields exceeded the moderate salinity threshold, indicating that while salinization is present, it remains in early stages. The NDSI approach proved effective for surface salinity detection, capturing both temporal fluctuations and spatial heterogeneity. These findings underscore the utility of remote sensing for operational salinity monitoring and highlight the importance of continuous observation to inform timely land management interventions. This study offers actionable insights for sustainable agriculture, particularly in tailoring irrigation and drainage strategies to mitigate salinity risks across vulnerable farmlands in Central Asia.

**Keywords:** land degradation, soil salinity, electrical conductivity, remote sensing, satellite images, normalized difference salinity index, spatiotemporal dynamics.

# 1. Introduction

Soil salinization is a severe form of land degradation that threatens agricultural productivity and ecosystem health worldwide. Traditional methods of mapping soil salinity rely on extensive ground sampling and laboratory analysis, which are labor-intensive, costly, and impractical for large areas. In recent years, remote sensing satellites coupled with machine learning have emerged as efficient tools for assessing and mapping soil salinity across wide regions [1, 2]. Optical sensors (Landsat, Sentinel-2) and radar sensors (Sentinel-1) can detect spectral and backscatter signatures related to surface salt content, while ML algorithms can learn complex relationships between signatures and ground-measured salinity.

Multi-spectral optical imagery and radar imagery are widely used to detect salinity-induced

signals on the soil surface. Salt-affected soils often exhibit characteristic spectral signatures, such as high reflectance in visible and near-infrared bands or distinctive vegetation stress signals. Many studies derive spectral indices to enhance salinity detection. For example, researchers in the Great Hungarian Plain [3] (Eastern Europe) used Landsat 8 to compute vegetation and salinity indices (along with principal components and land surface temperature) as inputs to regression models. In arid regions of Abu Dhabi, indices like NDVI (Normalized Difference Vegetation Index) and BSI (Bare Soil Index) showed moderate correlation with soil electrical conductivity, and their combination improved salinity prediction models [4]. Such indices capture reduced vegetation vigor or exposed bright soils typical of saline areas. However, optical methods have limits: heavy vegetation can mask soil signals, and beyond the top ~5 cm of soil, optical



reflectance is less sensitive to salt content [5]. To address this, some studies incorporate thermal infrared data (sensitive to soil moisture and salinity effects) or hyperspectral imagery for more diagnostic spectral features, though these data are less commonly available.

Central Asia has been a focal point for salinity research due to intensive irrigation desertification. Mukhamediev et al. mapped soil salinity across Turkestan, Almaty, Zhambyl, and Kyzylorda using a fusion of Sentinel-1 SAR and Landsat optical data, combined with machine learning models [6]. Their approach – employing boosted regression trees (XGBoost/LightGBM) outperformed models using optical data alone, showing better agreement with ground EC measurements. Using explainable ML, they also optimized feature selection without reducing accuracy. Notably, their regional model outperformed a global salinity model, highlighting the importance of local calibration. Merembayev et al. studied salinity in arid irrigated farms using highresolution radar textures and ML [7]. They highlighted strong spatial heterogeneity in salinity due to variable soil and irrigation conditions, which complicates mapping efforts. Their results showed that careful data partitioning and maintaining representative value distributions were key for model performance. LightGBM and Ridge regression achieved the best results ( $R^2 \sim 0.68$ ). The authors suggest future work should explore deep learning and physics-based models to enhance accuracy.

Researchers in [8] assessed soil salinity changes under climate change in the Khorezm region of Uzbekistan – an area with extensive irrigation. Their analysis noted that over the last 40 years, soil salinity has increased due to rising temperatures and poor drainage, and using saline groundwater for irrigation has exacerbated secondary salinization. By integrating remote sensing with climate data, they linked periods of warming and reduced river inflows to spikes in soil salt levels, predicting that climate change will continue to aggravate salinity unless irrigation management improves. A broader scale analysis by [9] provides a striking forecast for Central Asia. Using an automated ML framework to analyze drivers of salinity across Central Asia and neighboring Xinjiang (western China), they found that meteorological factors (aridity, temperature) exert the strongest influence on soil salt content, often interacting with landscape position (e.g. lowlying basins). Their model projected that with extreme climate warming scenarios, average soil salt concentrations could rise by about +21% in Central Asia by 2100, and as much as +65% in Xinjiang. Areas around irrigation water sources and topographic low points are at highest risk of salinity escalation. This study's methodology – using ML to parse out interaction effects between climate, topography, and human factors – is an innovative approach to understand spatio-temporal dynamics. It provides a quantitative glimpse into the future, highlighting that without intervention, Central Asia's salinization will intensify under climate change.

A major advantage of satellite-based monitoring is the ability to track salinity changes over time capturing both seasonal fluctuations and long-term trends. Historically, most remote sensing salinity studies focused on mapping spatial patterns at a single time, often neglecting the temporal dimension [10]. Recent work is beginning to fill this gap by leveraging multi-temporal image series and timeseries analysis. In irrigated areas, soil salinity fluctuates seasonally-often rising during dry periods due to evaporation and decreasing after rain or irrigation. Dense time-series from Sentinel-2 have been used to detect such patterns. For instance, [11] identified higher salinity in the dry season in China's Ebinur Lake wetland using RF models. Similarly, a study in the Werigan-Kuqa Oasis [12] found salinity shifts linked to precipitation variability, with expansion during droughts and retraction in wetter years. Multi-date imagery reduces noise and improves model accuracy. Duan et al. proposed a "combined-temporal" approach using multiple Sentinel-2 images around the sampling date [13]. This stabilized spectral signatures and improved model performance ( $R^2 = 0.72$ , RMSE  $\approx 0.87$  dS/m). However, salinity signals are affected by vegetation phenology and cropping cycles, necessitating integration with seasonal land cover and crop type data.

Comparing salinity maps over years reveals degradation or improvement patterns. In Zaghouan, Tunisia, salinized areas expanded from 2000 to 2023, linked to reduced rainfall and land use change ( $r \approx -0.85$  with precipitation), highlighting climate change as a key driver [13]. In contrast, the Xinjiang Oasis saw a salinity decline over 25 years, with nonsalinized land increasing and severe salinity retreating due to improved irrigation and drainage. Evidence from Iran's Golestan Province also

showed salinity reduction after drainage system installation, confirmed via satellite data. Meanwhile, in Central Asia's Kashgar region [14], time-series analyses revealed worsening salinity due to reclamation without drainage—mirroring issues in the Aral Sea basin.

A few studies directly compared different remote sensing approaches for mapping soil salinity under various environmental conditions. For instance, [15] compared Sentinel-2 vs Landsat-8 imagery for salinity mapping in a Mediterranean site, finding Sentinel-2's higher resolution gave it an edge in detecting fine-scale salinity patches. Conversely, another study in a Chinese wetland found Landsat-8's inclusion of a thermal band (absent in Sentinel-2) made it slightly superior for salinity estimation using a cubist model [16]. Such comparisons suggest that the "best" satellite platform may vary with context – Sentinel-2 excels with spatial detail and revisit frequency, whereas Landsat's thermal data can help in humid areas where evapotranspiration differences are key. In practice, many studies now use both (taking advantage of the combined 5-day revisit of Sentinel-2 and Landsat-8). On the ML side, comparisons like those by [17] in GEE have provided valuable guidance – they noted that while a CART model achieved the lowest error on training data, it tended to overfit extreme salinity, whereas RF provided more reliable generalization across landscapes. This hints that for operational mapping, a slightly less "accurate" but more stable model (RF) may be preferable to avoid speckled or noisy salinity maps.

Reliable ML modeling hinges on quality ground truth data, yet in many regions soil salinity sampling is sparse and infrequent due to the costs and effort required [18]. Small sample sizes can lead to unstable models. Most remote sensing methods primarily sense surface salt. This is problematic because harmful salinity can build up below the topsoil and escape detection until it surfaces [19, 20]. There is consensus that passive optical methods alone cannot fully capture subsoil salinity – thus, research is heading toward combining satellite data with geophysical surveys (EM induction, resistivity) or soil hydraulic models to infer salt distribution in

the profile. Thus, despite existing advances, using remote sensing or machine learning in isolation often faces limitations – such as sensitivity to seasonal variability, limited model transferability, or instability in interpreting temporal signals. The present study is aimed at assessing the spatial and temporal dynamics of soil salinity within the selected territory in the period from March to November. Based on the interpretation of satellite images and data processing in the GIS environment, an analysis of salinity changes has been performed, which allows not only to identify seasonal trends, but also to justify the need for sustainable approaches to land management.

### 2. Materials and methods

The study was conducted in the agricultural of Alakol District, Zhetisu Kazakhstan, encompassing a semi-arid continental environment. The area lies approximately between 46°N and 81°E (near Lake Alakol's basin), characterized by hot, dry summers and cold winters . Annual precipitation is low ( $\approx$ 150–280 mm), with most rain falling in spring (April-May) and late autumn. This climate and intensive irrigation practices make the region prone to soil salinization. as evaporation often exceeds rainfall, leading to salt accumulation at the surface. Thirty-one sampling sites were selected across the district's farmlands to capture spatial variability. At each site, we collected surface soil samples and measured electrical conductivity in a 1:5 soil-water extract as a ground truth indicator of salinity. The EC values ranged from 0.07 (non-saline) up to 1.4 (highly saline) in the 1:5 extract. We also recorded terrain attributes at each site: elevation (from a DEM), local slope, and ambient surface temperature. Elevations spanned ~379–495 m above sea level (lower toward the lake plain, higher in uplands), and slopes were gentle (mostly <1° incline). Notably, the lowest-lying fields tended to have higher measured salinity, consistent with salt accumulation in topographic depressions. Table 1 summarizes the field data, including coordinates, electrical conductivity (EC), elevation, surface temperature, and slope values for each of the 31 sampling sites.

Table 1 – Field data

Field №	X	Y	EC (1:5), dS/m	DEM, m	Surface temp., °C	Slope
ALK1	81.263687	46.013337	0.16	387	42.35	0.8863131403923035
ALK2	81.263322	46.013021	0.2	387	42.35	0.8863131403923035
ALK3	81.262991	46.012058	0.44	387	42.35	0.8863131403923035
ALK4	81.252822	46.014737	0.15	386	42.78	0.4236890375614166
ALK5	81.252683	46.014185	0.48	386	42.78	0.4236890375614166
ALK6	81.258905	46.033323	0.35	380	39.97	0.41753801703453064
ALK7	81.262467	46.033464	0.52	380	39.16	0.41753801703453064
ALK8	81.235861	46.061892	0.37	396	39.55	0.5087683796882629
ALK9	81.236126	46.062183	0.38	396	39.55	0.5087683796882629
ALK10	81.227602	46.09355	0.19	395	41.56	0.5410060882568359
ALK11	81.226884	46.093285	0.13	395	41.56	0.5410060882568359
ALK12	81.20694	46.153272	0.34	369	40.9	0.272049218416214
ALK13	81.184885	46.143835	0.4	384	39.91	0.49335935711860657
ALK14	81.175125	46.125639	0.73	401	40.55	0.5325705409049988
ALK15	81.183753	46.120222	0.46	404	41.21	0.5124315023422241
ALK16	81.184296	46.120402	0.41	404	41.21	0.5124315023422241
ALK17	81.15495	46.164803	0.22	382	37.76	0.4547281265258789
ALK18	81.155732	46.165621	0.21	382	37.76	0.4547281265258789
ALK19	81.155817	46.165726	0.21	382	37.76	0.4547281265258789
ALK20	81.045543	46.194957	0.22	379	39.85	0.30169597268104553
ALK21	81.046017	46.194684	0.21	379	39.76	0.30169597268104553
ALK22	80.988318	46.183279	0.21	390	40.75	0.43475303053855896
ALK23	80.988355	46.183294	0.21	390	40.75	0.43475303053855896
ALK24	80.830143	46.244836	0.2	381	44.13	0.13844919204711914
ALK25	80.829652	46.212158	0.07	384	45.57	0.17097853124141693
ALK26	80.829596	46.213915	0.08	384	45.57	0.17097853124141693
ALK27	80.829592	46.213916	1.4	384	45.57	0.17097853124141693
ALK28	81.054566	46.069562	0.36	495	40.66	0.5086142420768738
ALK29	81.099052	46.036487	0.53	492	41.56	0.5497124791145325
ALK30	81.100584	46.036445	0.47	492	40.5	0.5497124791145325
ALK31	81.101486	46.036861	0.38	492	40.5	0.5497124791145325

Fig. 1 presents the collected soil samples, which were used for laboratory measurement of electrical conductivity (EC) as ground-truth data.

Fig. 2 shows the geographical location of the study area within Alakol District, Zhetisu region, including the spatial distribution of sampling sites.

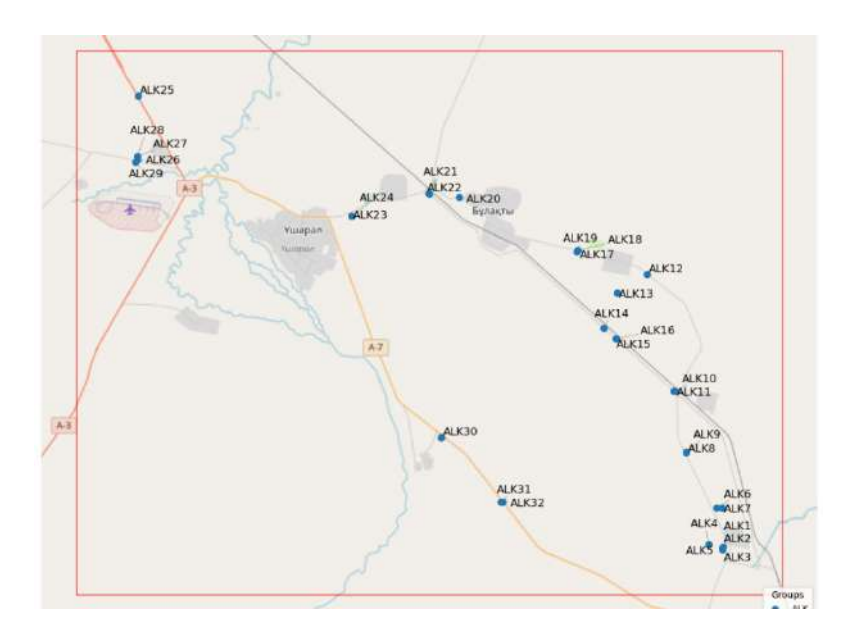


Figure 1 – Soil samples collected from agricultural fields



Figure 2 – Location of the study area and distribution of field sampling sites

To monitor salinity dynamics over the 2024 growing season, we acquired Sentinel-2 MultiSpectral Instrument (MSI) imagery for each month from March through November (one cloud-free scene per month). Sentinel-2 provides 13 spectral bands, including visible, near-infrared (NIR), and shortwave-infrared (SWIR)

wavelengths, at spatial resolutions of 10–20 m, with a 5-day revisit frequency. We downloaded Level-2A surface reflectance products (which are already atmospherically corrected to bottom-of-atmosphere reflectance) covering the study area. Each monthly image was projected to the WGS 84 / UTM Zone 44N coordinate system and clipped to the

boundaries of the target agricultural fields. Cloud masking was applied using the Sentinel-2 Scene Classification Layer (SCL) to remove cloud- and shadow-affected pixels. We ensured minimal cloud cover by selecting images on or near clear-sky dates for each month; if the primary monthly image had cloud contamination, an alternate cloud-free image from the same month was used. This preprocessing workflow yielded a time-series of nine cloud-free reflectance maps (March-November 2024) for the region. All images were co-registered to ensure that multi-date pixel-wise comparisons were spatially consistent, and radiometric consistency was maintained by using the atmospherically corrected reflectances (ensuring comparability across dates). We also extracted reflectance and index values at the 31 field sampling locations for each date to facilitate direct comparison with ground measurements of salinity. Fig. 3 illustrates the sequential workflow for mapping soil salinity using Sentinel-2 satellite imagery. The process comprises six main stages:

- High-resolution multispectral imagery from Sentinel-2 is acquired for the area of interest. These data provide the necessary spectral information to detect surface-level variations in soil properties, including salinity.
- Specific spectral bands (such as the Red, Green, and Near Infrared (NIR) bands) are selected based on their sensitivity to soil salinity and moisture content. These bands serve as the input for index-based salinity assessments.
- The selected images undergo preprocessing steps, including atmospheric correction, resampling, and cropping. The cropping operation ensures that the imagery conforms to the boundaries of the study area, facilitating localized analysis.

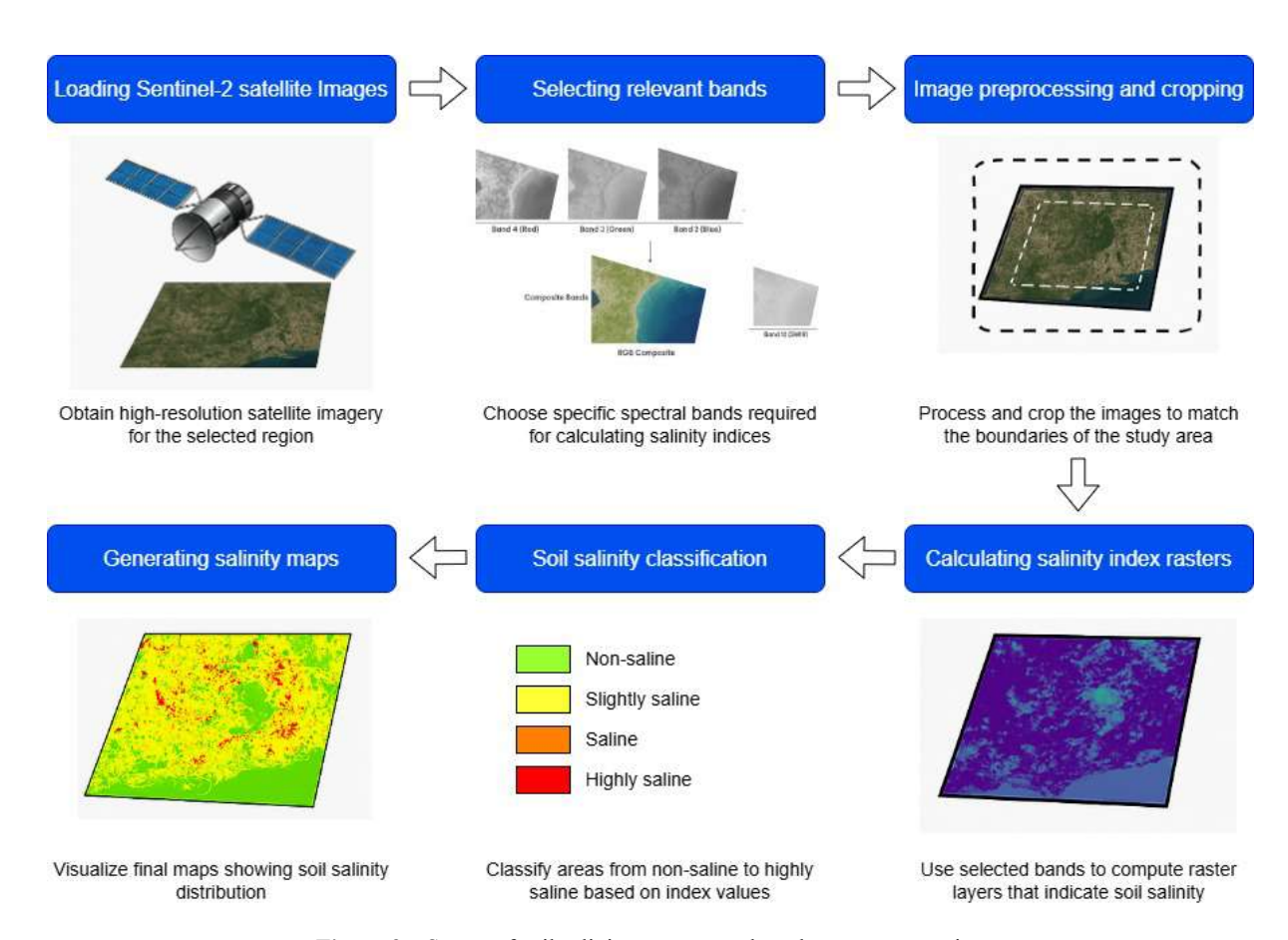


Figure 3 – Stages of soil salinity assessment based on remote sensing

- Using the relevant bands, salinity indices are computed to generate raster layers. These layers

indicate spatial variations in soil salinity levels based on spectral reflectance properties.

- The index values are classified into predefined salinity categories (non-saline, slightly saline, moderate saline, and highly saline). This classification supports the interpretation and evaluation of salinity severity across the landscape.
- The final classified raster outputs are visualized as salinity maps.

## 3. Results

The NDSI analysis from March to November 2024 shows clear temporal and spatial patterns of

soil salinity across the study area. To interpret the index values, we categorised NDSI into four classes: non-saline, slightly saline, moderately saline and highly saline (Table 2).

The NDSI was calculated using the spectral bands Red (Band 4) and Near-Infrared (NIR, Band 8) from Sentinel-2 imagery [21]:

$$NDSI = \frac{(Red-NIR)}{(Red+NIR)}$$
 (1)

Across all nine months, the observed NDSI values ranged approximately from -0.58 to -0.03 (Table 3).

Table 2 – Soil salinity classification.

Categories	EC(1:5)	NDSI		
Non-saline	<0,16	<0,2		
Slightly saline	0,16≤x<0,22	-0,2≤x<0		
Moderately saline	0,22≤x<0,74	0≤x<0,2		
Highly saline	≥0,74	≥0,2		

**Table 3** – Normalized difference salinity index measurements.

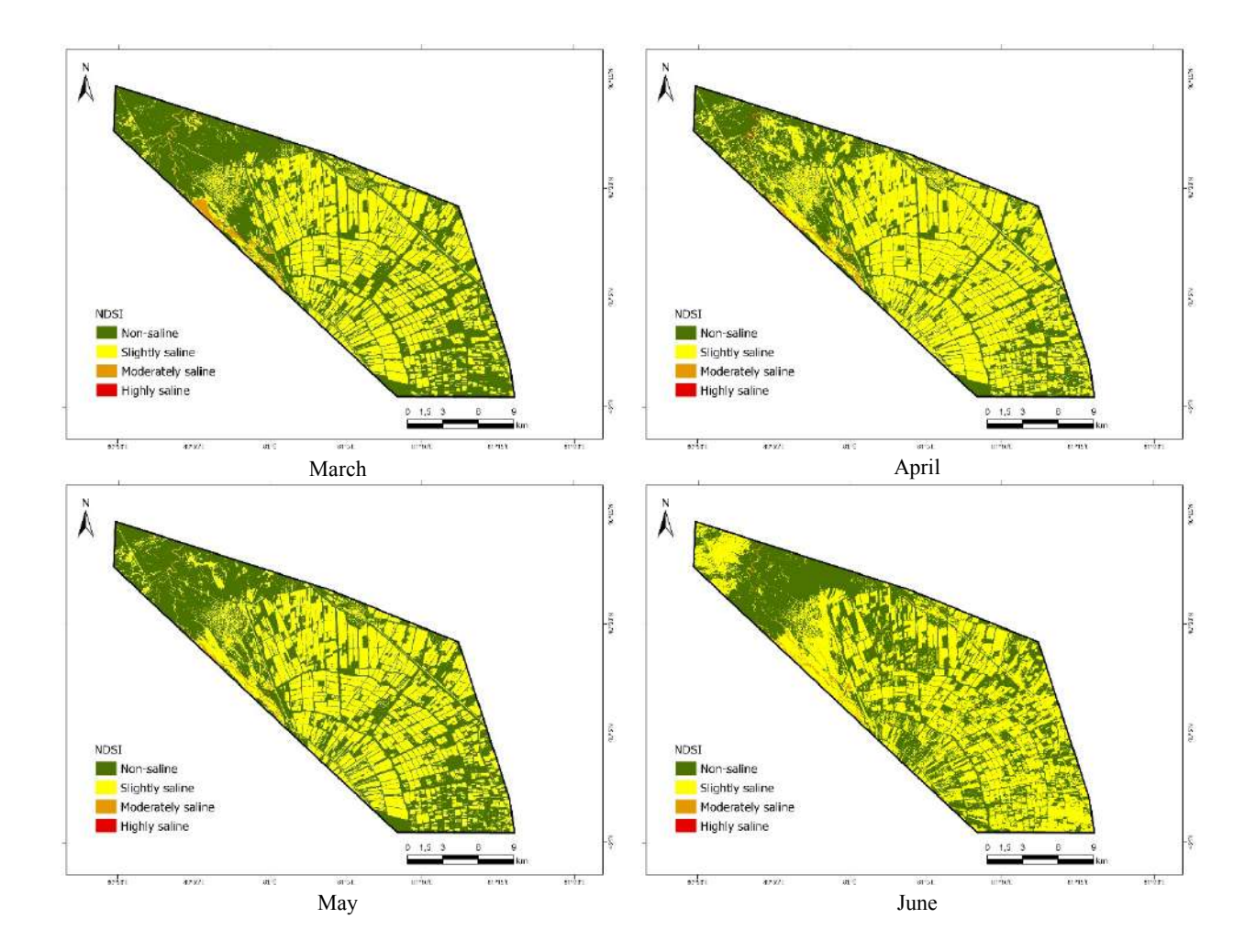
E' . L J. NC	NDSI								
Field №	Mar	Apr	May	Jun	Jul	Aug	Sep	Oct	Nov
ALK1	-0,171	-0,272	-0,295	-0,184	-0,130	-0,121	-0,144	-0,126	-0,112
ALK2	-0,145	-0,208	-0,247	-0,161	-0,107	-0,094	-0,102	-0,099	-0,113
ALK3	-0,112	-0,207	-0,223	-0,224	-0,171	-0,107	-0,114	-0,101	-0,10
ALK4	-0,117	-0,180	-0,093	-0,105	-0,178	-0,578	-0,532	-0,220	-0,07
ALK5	-0,128	-0,195	-0,150	-0,222	-0,282	-0,406	-0,493	-0,258	-0,11
ALK6	-0,128	-0,264	-0,364	-0,367	-0,448	-0,457	-0,509	-0,367	-0,11
ALK7	-0,098	-0,122	-0,103	-0,175	-0,252	-0,478	-0,373	-0,264	-0,14
ALK8	-0,132	-0,268	-0,309	-0,430	-0,481	-0,364	-0,286	-0,194	-0,11
ALK9	-0,101	-0,146	-0,171	-0,285	-0,292	-0,221	-0,253	-0,172	-0,09
ALK10	-0,169	-0,267	-0,289	-0,163	-0,112	-0,149	-0,220	-0,193	-0,05
ALK11	-0,081	-0,135	-0,158	-0,101	-0,521	-0,520	-0,297	-0,346	-0,12
ALK12	-0,090	-0,193	-0,232	-0,322	-0,308	-0,326	-0,316	-0,178	-0,08
ALK13	-0,104	-0,147	-0,197	-0,086	-0,304	-0,215	-0,106	-0,106	-0,10
ALK14	-0,083	-0,182	-0,163	-0,208	-0,198	-0,221	-0,129	-0,116	-0,03
ALK15	-0,138	-0,247	-0,280	-0,226	-0,126	-0,113	-0,150	-0,134	-0,07
ALK16	-0,183	-0,291	-0,284	-0,170	-0,121	-0,115	-0,140	-0,130	-0,12
ALK17	-0,110	-0,095	-0,242	-0,140	-0,116	-0,133	-0,177	-0,164	-0,13
ALK18	-0,078	-0,128	-0,100	-0,201	-0,403	-0,449	-0,420	-0,189	-0,05
ALK19	-0,078	-0,128	-0,100	-0,201	-0,403	-0,449	-0,420	-0,189	-0,05
ALK20	-0,079	-0,090	-0,160	-0,271	-0,398	-0,268	-0,231	-0,157	-0,06
ALK21	-0,064	-0,112	-0,135	-0,242	-0,427	-0,356	-0,162	-0,152	-0,10
ALK22	-0,201	-0,330	-0,391	-0,247	-0,168	-0,137	-0,137	-0,116	-0,18
ALK23	-0,117	-0,266	-0,485	-0,457	-0,189	-0,118	-0,125	-0,118	-0,15
ALK24	-0,162	-0,253	-0,283	-0,229	-0,217	-0,238	-0,246	-0,196	-0,18
ALK25	-0,203	-0,288	-0,295	-0,267	-0,214	-0,181	-0,176	-0,139	-0,053

Continuation of the table

Field №	NDSI								
riela M	Mar	Apr	May	Jun	Jul	Aug	Sep	Oct	Nov
ALK26	-0,185	-0,273	-0,232	-0,190	-0,143	-0,133	-0,145	-0,122	-0,120
ALK27	-0,185	-0,273	-0,232	-0,190	-0,143	-0,133	-0,145	-0,122	-0,120
ALK28	-0,107	-0,096	-0,066	-0,236	-0,253	-0,173	-0,133	-0,107	-0,136
ALK29	-0,088	-0,135	-0,186	-0,193	-0,140	-0,106	-0,109	-0,105	-0,124
ALK30	-0,068	-0,108	-0,142	-0,101	-0,072	-0,056	-0,095	-0,077	-0,081
ALK31	-0,155	-0,212	-0,215	-0,138	-0,109	-0,089	-0,096	-0,091	-0,097

Notably, almost none of the sampled locations exceeded an NDSI of 0, meaning moderate or high salinity levels were not reached in surface reflectance during 2024. Instead, most values fell in

the non-saline or slightly saline categories. Figure 4, which displays monthly salinity maps, visually corroborates these findings by illustrating the expansion and contraction of saline areas over the seasons.



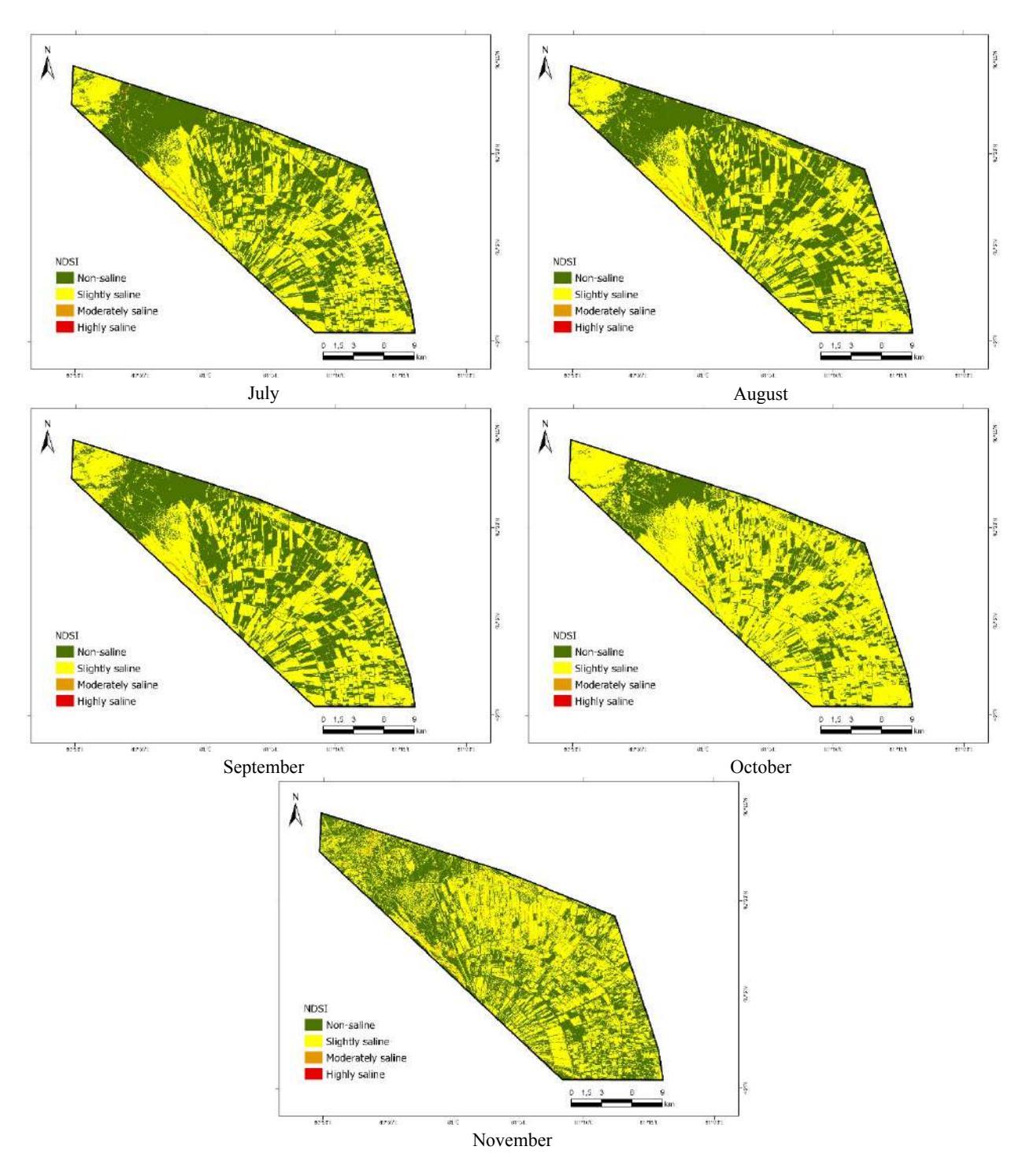


Figure 4 – Soil salinity distribution maps

- In early spring (March–April), soil salinity was generally low. March NDSI values averaged around -0.15 to -0.20 in many fields. By April, additional rainfall and early irrigation likely leached some surface salt, resulting in even more negative

NDSI values in several fields. Many sites in April and May recorded NDSI below -0.2. This period represents the annual minimum for surface salinity; the land had been flushed by spring moisture, leaving little salt at the surface. For instance, ALK5

had an NDSI of -0.30 in May, compared to -0.16 in March – a drop indicating reduced salinity as spring progressed.

- Moving into summer, the trend reverses. By June, as temperatures rose and soils began drying, NDSI values in many fields started to increase, signaling a resurgence of salinity at the surface. The peak of summer (July-August) showed the most significant salinity levels. During July, a majority of fields shifted into the slightly saline category. By August, nearly all fields exhibited higher NDSI compared to spring: values commonly ranged from about -0.15 up to -0.08. A few fields even approached the threshold of moderate salinity – for example, one low-lying field reached an NDSI of – 0.05 in August, the highest value observed. Although these values remained just below zero, indicate that salts had considerably accumulated on the soil surface by late summer.
- In the autumn months (September-November). salinity levels exhibited slight improvements in some fields, while others remained high. September's NDSI values were still elevated (mostly in the -0.1 to -0.18 range), not significantly different from August in many cases. However, by October, a modest decrease in salinity is evident in a number of fields: for instance, fields that had NDSI around -0.10 in late summer dropped to approximately -0.13 to -0.15 in October. This suggests that as temperatures fell and crop water use declined, there was less evaporation to concentrate salts, and any early autumn rainfall may have begun to dissolve or move salts downward.
- By November, a few fields continued to show some of the highest salinity readings of the year (NDSI  $\approx -0.05$  to -0.08, remaining in the slightly saline class despite the season), especially those that are poorly drained. In other fields,

November brought further slight decreases in NDSI (down to  $\sim$ -0.18 to -0.20), nearly returning to springtime non-saline levels.

To assess the validity of the NDSI satellite indicator, a correlation analysis was performed using the Pearson correlation coefficient between EC and NDSI [22]:

$$r = \frac{\sum_{i=1}^{n} (x_i - \bar{x})(y_i - \bar{y})}{\sqrt{\sum_{i=1}^{n} (x_i - \bar{x})^2 \cdot \sqrt{\sum_{i=1}^{n} (y_i - y)^2}}}$$
(2)

where  $x_i$  – EC value for i field,

 $y_i$  – NDSI value for i field,

 $\bar{x}$  – average EC value,

 $\bar{y}$  – average NDSI value.

To estimate how much the observed value deviates from the expected value, if the null hypothesis is correct, we will calculate the t-statistics:

$$t = \frac{r \cdot \sqrt{n-2}}{\sqrt{1-r^2}} \tag{3}$$

After calculating t, this value will be compared with the Student's distribution (t-distribution) with df = n-2:

$$p = 2 \cdot (1 - T_{CDF}(|t|, df))$$
 (4)

 $T_{CDF}$  – cumulative distribution function, df = n-2

The calculation results are shown in Table 4. There is a weak but positive relationship between the EC and NDSI values, which gives the right to use NDSI as a reliable indicator of salinity for monitoring large areas without the need for continuous sampling. Non-simultaneous measurements are a limitation for calculations, since the EC is taken at one moment, and the NDSI changes monthly.

Table 4 – NDSI	satellite indicator	validity	assessment.
I abic T - NDSI	satemite mulcator	vanuity	assessificit.

Month	r	t	p-value	Interpretation
March	-0.0047	-0.025	0.980	No connection
April	-0.0260	-0.140	0.889	No connection
May	+0.1128	+0.611	0.546	Weak positive connection
June	+0.0494	+0.266	0.792	No connection
July	+0.1889	+1.036	0.309	Weak positive connection
August	+0.1775	+0.972	0.339	Weak positive connection
September	+0.1563	+0.852	0.401	Weak positive connection
October	+0.1673	+0.914	0.368	Weak positive connection
November	+0.0147	+0.079	0.938	No connection

Superimposed on these temporal trends are distinct spatial patterns in salinity. Certain fields consistently showed higher salinity than others, underlining the role of site-specific factors. In particular, fields situated at lower elevations or poorly drained positions were much more prone to salinisation. For example, ALK27 (located in a topographic depression near the lake plain) had NDSI values of approximately -0.28 in May (virtually non-saline after spring rains) but rose to around -0.06 by November, categorising it as one of the most saline fields by year's end. In contrast, ALK28, which lies on higher ground, ranged from about -0.25 (May) to -0.12 (August), never exceeding the slightly saline range and ending the season near -0.18 in November. This comparison illustrates that the low-lying field accumulated and retained far more salt over the season than the upland field. Such patterns were typical: nearly all the lowest-lying fields had the highest salinity readings, whereas fields at higher elevations or with better natural drainage remained relatively less affected. This observation aligns with the ground truth data, which showed that the lowest elevation sites had the highest soil EC measurements.

Series of maps in Fig. 4 highlights these spatial differences – the same areas (notably, the northern and central parts of the district closer to Lake Alakol) repeatedly show up as saline-hued zones in summer and autumn, whereas southern and higher-elevation plots stay blue (non-saline) throughout.

# 4. Discussion

The spatio-temporal patterns observed in this study reflect the interplay of climatic, hydrological, and land-use factors characteristic of semi-arid irrigated environments. During spring, precipitation and irrigation water dilute and leach salts from the topsoil, whereas in summer, high evaporation rates draw moisture up, causing dissolved salts to crystallise at the surface [23, 24]. Our results confirm this cycle - the pronounced increase in salinity from May to August indicates evaporative salt concentration under hot, dry conditions. By late autumn, the slight reductions in NDSI in some fields suggest that cooler temperatures and occasional rain may have partially re-dissolved surface salts. However, the fact that many fields remained more saline in November than in March implies that seasonal flushing was incomplete. In practice, this means salts can carry over into the next year, leading to a gradual buildup if not managed. Thus, even though salinity may appear to recede each spring, the summer accumulations pose a recurring stress that can contribute to long-term soil degradation if proper remediation is not in place.

Topography and water flow emerge as critical drivers of the spatial salinity patterns [25]. Fields in depressions or near the lake plain consistently showed higher salinity, which is consistent with water pooling and evaporating in these low-lying areas, leaving behind salt deposits. In contrast, fields on slight rises or with better drainage had lower NDSI values, as excess water (and salt) could more easily percolate away. This observation corresponds with well-known behaviour of salts accumulating in landscape low points. Similar findings have been reported in other Central Asian studies [8, 9] – for instance, a regional analysis noted that areas around irrigation water sources and topographic low points are at highest risk of salinity escalation. Our fieldscale heterogeneity (where adjacent fields had quite different salinity levels) also echoes the work of [7], who found strong spatial variability in salinity due to differences in soil properties and irrigation practices even within a small area. Such comparisons highlight that local factors (microrelief, irrigation scheduling, soil texture, etc.) can cause significant divergence in salinity outcomes, underlining the importance of site-specific management strategies. Regarding the efficacy of the NDSI approach, our use of a simple spectral index proved effective in capturing surface salt dvnamics.

The temporal trends in NDSI aligned with expected seasonal salinity changes and qualitatively matched ground EC data-fields with higher EC generally showed less negative NDSI values. This confirms NDSI's usefulness as a rapid, costeffective tool for surface salinity monitoring. Its sensitivity enabled detection of subtle monthly variations and emerging salinity hotspots. However, NDSI reflects only surface conditions and can be influenced by vegetation or soil moisture. In areas dense crop cover, salinity may underestimated due to spectral masking. Moreover, similar reflectance can result from dry soil or carbonates, reducing specificity. In this study, the predominantly bare fields enhanced the reliability of NDSI, though its effectiveness may decline in heavily vegetated areas.

Another limitation of NDSI is its inability to detect subsurface salinity–salts beneath a thin

surface layer may go unnoticed until they re-emerge. To address this, integrating radar data (e.g., Sentinel-1) can improve detection, as radar is sensitive to surface roughness and moisture and is unaffected by vegetation cover. Studies in Kazakhstan confirm that combining optical and radar imagery enhances salinity mapping accuracy [6, 7]. Thermal infrared data could also help by revealing moisture and evaporation patterns linked to salinity. Additionally, machine learning models that integrate multiple indices and auxiliary data (e.g., terrain, climate) can improve prediction. While NDSI was effective for surface monitoring in this study, a multi-source, multi-index approach would offer a more comprehensive assessment.

#### 5. Conclusion

This study provided a detailed spatio-temporal assessment of soil salinity in irrigated agricultural lands of Alakol District, Kazakhstan, using timeseries Sentinel-2 imagery. By tracking the NDSI over the 2024 growing season (March to November), we identified clear seasonal patterns: salinity was lowest in spring after winter and early rains, increased markedly in summer due to evaporation and irrigation practices, and persisted into autumn to varying degrees across the landscape. Spatial analysis further revealed that salinity issues are concentrated in specific areas - notably, lowlying fields near the lake basin experienced the greatest salt accumulation, whereas upland fields were relatively less affected. Importantly, the salinity levels observed (as indicated by NDSI) remained in the slight to moderate range, with no extreme salinity outbreaks during the study period. This suggests that while salinisation is a concern, it may still be at a manageable stage if addressed promptly. The findings underscore the importance of monitoring soil salinity over time. A one-off measurement provides only a snapshot; in contrast, the temporal approach adopted here captures the dynamic nature of salinity, revealing when peaks occur and when remediation would be most needed.

Although the statistical correlation between the Normalized Difference Salinity Index (NDSI) and field-measured electrical conductivity (EC) was modest, the index effectively captured distinct seasonal and spatial patterns of soil salinity. Given the limitations in ground data frequency and temporal alignment, NDSI values should not be interpreted in absolute terms. Instead, they should be regarded as qualitative indicators of salinity variation, capable of supporting spatiotemporal monitoring and the identification of emerging salinity hotspots. Future research should aim to improve ground validation protocols through more frequent and temporally aligned EC sampling and explore the integration of NDSI with complementary data sources-such as radar imagery, soil moisture metrics, and topographic parameters using hybrid or machine learning-based models to enhance the accuracy and robustness of salinity assessments.

# **Funding**

This research was funded by the Science Committee of the Ministry of Science and Higher Education of the Republic of Kazakhstan grant number AP23488281.

# **Author Contributions**

Conceptualization, A.A. and M.T.; Methodology, A.A. and M.T.; Software, A.A. and M.T.; Validation, A.A. and M.T.; Formal Analysis, A.A.; Investigation, A.A. and M.T.; Resources, A.A. and M.T.; Data Curation, A.A. and M.T.; Writing – Original Draft Preparation, A.A.; Writing – Review & Editing, A.A. and M.T.; Visualization, A.A.; Supervision, M.T.; Project Administration, M.T.; Funding Acquisition, M.T.

# **Conflicts of Interest**

The authors declare no conflict of interest.

## References

- 1. S.K. Sarkar, R. Rudra, A. Reza, P. Das and A. Islam, "Coupling of machine learning and remote sensing for soil salinity mapping in coastal area of Bangladesh," *Scientific Reports*, vol. 13, 2023. doi: 10.1038/s41598-023-44132-4.
  - 2. R. Taghizadeh-Mehrjardi, "Sentinel-2 and Ensemble ML for Soil Salinity Mapping in Iran," Geoderma, vol. 409, 2022.
- 3. G. Sahbeni, "Soil salinity mapping using Landsat 8 OLI data and regression modeling in the Great Hungarian Plain." *Applied Sciences*, vol. 3, no. 587, 2021. doi: 10.1007/s42452-021-04587-4.
- 4. A.S. Alqasemi, M. Ibrahim, A.Q. Fadhil and G. Kaplan, "Detection and modeling of soil salinity variations in arid lands using remote sensing data," *Open Geosciences*, vol. 13, no. 1, 2021, pp. 443-453. doi: 10.1515/geo-2020-0244.
- 5. F. Wang et al., "Advancements and perspective in the quantitative assessment of soil salinity utilizing remote sensing and machine learning algorithms: A review," *Remote Sens.*, vol. 16, no. 24, p. 4812, 2024, doi: 10.3390/rs16244812.
- 6. R. I. Mukhamediev et al., "Soil salinity estimation for South Kazakhstan based on SAR Sentinel-1 and Landsat-8,9 OLI data with machine learning models," *Remote Sens.*, vol. 15, no. 17, p. 4269, 2023, doi: 10.3390/rs15174269.
- 7. Y. Amirgaliyev, R. Mukhamediev, T. Merembayev et al., "Remote sensing and machine learning algorithms to predict soil salinity in southern Kazakhstan," *Discover Sustainability*, vol. 5, p. 363, 2024, doi: 10.1007/s43621-024-00594-8.
- 8. M. Khamidov, J. Ishchanov, A. Hamidov, C. Donmez, and K. Djumaboev, "Assessment of soil salinity changes under the climate change in the Khorezm region, Uzbekistan," Int. J. Environ. Res. *Public Health*, vol. 19, no. 14, p. 8794, 2022, doi: 10.3390/ijerph19148794.
- 9. L. Wang et al., "An automated framework for interaction analysis of driving factors on soil salinization in Central Asia and Western China," *Remote Sens.*, vol. 17, no. 6, p. 987, 2025, doi: 10.3390/rs17060987.
- 10.Y. Zhang et al., "Mapping the soil salinity distribution and analyzing its spatial and temporal changes in Bachu County, Xinjiang, based on Google Earth Engine and machine learning," *Agriculture*, vol. 14, no. 4, p. 630, 2024, doi: 10.3390/agriculture14040630.
- 11. S. Bandak, S. A. Movahedi-Naeini, S. Mehri, and A. Lotfata, "A longitudinal analysis of soil salinity changes using remotely sensed imageries," *Sci. Rep.*, vol. 14, no. 1, p. 10383, May 2024, doi: 10.1038/s41598-024-60033-6.
- 12. S. Ma, B. He, B. Xie, X. Ge, and L. Han, "Investigation of the spatial and temporal variation of soil salinity using Google Earth Engine: a case study at Werigan-Kuqa Oasis, West China," *Sci. Rep.*, vol. 13, no. 1, p. 2754, Feb. 2023, doi: 10.1038/s41598-023-27760-8.
- 13. C. Duan, Y. Zhang, C. Hu, H. Chen, and P. Liu, "Soil salinity inversion by combining multi-temporal Sentinel-2 images near the sampling period in coastal salinized farmland," *Front. Environ. Sci.*, vol. 13, p. 1533419, 2025, doi: 10.3389/fenvs.2025.1533419.
- 14. N. Erkin et al., "Method for predicting soil salinity concentrations in croplands based on machine learning and remote sensing techniques," *J. Appl. Remote Sens.*, vol. 13, no. 3, pp. 034520–034520, 2019, doi: 10.1117/1.JRS.13.034520.
- 15. E. Davis, C. Wang, and K. Dow, "Comparing Sentinel-2 MSI and Landsat 8 OLI in soil salinity detection: A case study of agricultural lands in coastal North Carolina," *International Journal of Remote Sensing*, vol. 40, no. 16, pp. 6134–6153, 2019, doi: 10.1080/01431161.2019.1587205.
- 16. J. Wang et al., "Machine learning-based detection of soil salinity in an arid desert region, Northwest China: A comparison between Landsat-8 OLI and Sentinel-2 MSI," Sci. Total Environ., vol. 707, p. 136092, 2020, doi: 10.1016/j.scitotenv.2019.136092.
- 17. S. Aksoy et al., "Assessing the performance of machine learning algorithms for soil salinity mapping in Google Earth Engine platform using Sentinel-2A and Landsat-8 OLI data," *Adv. Space Res.*, vol. 69, no. 2, pp. 1072–1086, 2022, doi: 10.1016/j.asr.2021.10.024.
- 18. J. W. Sirpa-Poma et al., "Towards the improvement of soil salinity mapping in a data-scarce context using Sentinel-2 images in machine-learning models," *Sensors*, vol. 23, no. 23, p. 9328, Nov. 2023, doi: 10.3390/s23239328.
- 19. A. Bannari and Z. M. Al-Ali, "Assessing climate change impact on soil salinity dynamics between 1987–2017 in arid landscape using Landsat TM, ETM+ and OLI data," *Remote Sens.*, vol. 12, no. 17, p. 2794, 2020.
- 20. V. Habibi, H. Ahmadi, M. Jafari, and A. Moeini, "Mapping soil salinity using a combined spectral and topographical indices with artificial neural network," *PLoS One*, vol. 16, no. 5, 2021.
- 21. K.-A. Nguyen, Y.-A. Liou, P. Tran, H. P. Phung, and T.-H. Nguyen, "Soil salinity assessment by using near-infrared channel and Vegetation Soil Salinity Index derived from Landsat 8 OLI data: a case study in the Tra Vinh Province, Mekong Delta, Vietnam," *Prog. Earth Planet. Sci.*, vol. 7, 2020, doi: 10.1186/s40645-019-0311-0.
- 22. J. Ding, S. Yang, Q. Shi, Y. Wei, and F. Wang, "Using apparent electrical conductivity as indicator for investigating potential spatial variation of soil salinity across seven oases along Tarim River in Southern Xinjiang, China," *Remote Sens.*, vol. 12, p. 2601, 2020, doi: 10.3390/rs12162601.
- 23. N. E. Silvero et al., "Soil property maps with satellite images at multiple scales and its impact on management and classification," *Geoderma*, vol. 397, p. 115089, 2021.
- 24. A. S. Abuzaid et al., "Multi-indicator and geospatial based approaches for assessing variation of land quality in arid agroecosystems," *Sustainability*, vol. 14, p. 5840, 2022.
- 25. A. Okasha et al., "Effects of irrigation method and water flow rate on irrigation performance, soil salinity, yield, and water productivity of cauliflower," *Agriculture*, vol. 12, pp. 1–18, 2022, doi: 10.3390/agriculture12081164.

# Information about authors

Aisulu Ataniyazova — PhD student at Al-Farabi Kazakh National University, Faculty of Information Technologies (Almaty, Kazakhstan, aisulu.ataniyazova@gmail.com). Her research interests include machine learning and remote sensing. ORCID iD: 0000-0003-1122-6614.

Timur Merembayev – PhD, Research Assistant at the Institute of Information and Computational Technologies (Almaty, Kazakhstan, merembaevt@gmail.com). His current research covers various topics in a mathematical simulation of physical processes, machine learning, and geoscience problems. ORCID iD: 0000-0001-8185-235X.

Submission received: 18 April, 2025.

Revised: 28 May, 2025. Accepted: 28 May, 2025.